Cell Reports

Large Maf transcription factor family is a major regulator of fast type IIb myofiber determination

Graphical abstract

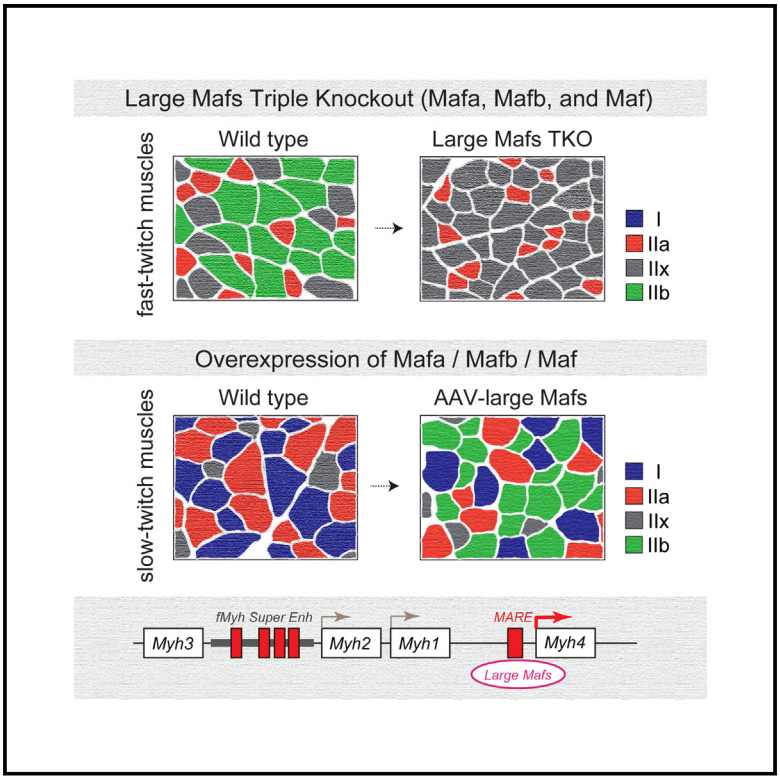

Highlights

- Large Mafs are predominantly expressed in fast-twitch skeletal muscles
- Large Maf ablation in skeletal muscle depletes fast type IIb myofiber content
- Large Mafs specifically bind to the Maf recognition elements of the *Myh4* promoter
- Overexpression of a large Maf induces fast type IIb myofibers in adult soleus muscle

Authors

Shunya Sadaki, Ryo Fujita, Takuto Hayashi, ..., Takashi Kudo, Shin'ichi Takeda, Satoru Takahashi

Correspondence

fujiryo@md.tsukuba.ac.jp (R.F.), satoruta@md.tsukuba.ac.jp (S.T.)

In brief

Sadaki et al. identify large Mafs as major regulators of type IIb myofiber specification. Large Maf-deficient skeletal muscles show severe loss of type IIb myofibers, with a myofiber type shift toward IIx/IIa. Conversely, single large Maf overexpression enhances type IIb myofiber formation through Maf recognition elements in the *Myh4* promoter.

Sadaki et al., 2023, Cell Reports *42*, 112289
April 25, 2023
https://doi.org/10.1016/j.celrep.2023.112289

CellPress

Cell Reports

CellPress
OPEN ACCESS

Report

Large Maf transcription factor family is a major regulator of fast type IIb myofiber determination

Shunya Sadaki,[1,2] Ryo Fujita,[3,10,*] Takuto Hayashi,[1,4] Ayano Nakamura,[5] Yui Okamura,[5] Sayaka Fuseya,[1] Michito Hamada,[1] Eiji Warabi,[1] Akihiro Kuno,[1] Akiko Ishii,[6] Masafumi Muratani,[7] Risa Okada,[8] Dai Shiba,[8] Takashi Kudo,[1] Shin'ichi Takeda,[9] and Satoru Takahashi[1,*]

[1]Laboratory Animal Resource Center in Transborder Medical Research Center, and Department of Anatomy and Embryology, Institute of Medicine, University of Tsukuba, Tsukuba, Ibaraki 305-8575, Japan
[2]Ph.D. Program in Humanics, School of Integrative and Global Majors, University of Tsukuba, Tsukuba, Ibaraki 305-8575, Japan
[3]Division of Regenerative Medicine, Transborder Medical Research Center, Institute of Medicine, University of Tsukuba, Tsukuba, Ibaraki 305-8575, Japan
[4]Doctoral Program in Biomedical Sciences, Graduate School of Comprehensive Human Sciences, University of Tsukuba, Tsukuba, Ibaraki 305-8575, Japan
[5]College of Medicine, School of Medicine and Health Sciences, University of Tsukuba, Tsukuba, Ibaraki 305-8575, Japan
[6]Department of Neurology, Institute of Medicine, University of Tsukuba, Tsukuba, Ibaraki 305-8575, Japan
[7]Department of Genome Biology, Transborder Medical Research Center, Institute of Medicine, University of Tsukuba, Tsukuba, Ibaraki 305-8575, Japan
[8]JEM Utilization Center, Human Spaceflight Technology Directorate, Japan Aerospace Exploration Agency (JAXA), Tsukuba, Ibaraki 305-8505, Japan
[9]Department of Molecular Therapy, National Institute of Neuroscience, National Center of Neurology and Psychiatry, 4-1-1 Ogawa-higashi, Kodaira, Tokyo 187-8502, Japan
[10]Lead contact
*Correspondence: fujiryo@md.tsukuba.ac.jp (R.F.), satoruta@md.tsukuba.ac.jp (S.T.)
https://doi.org/10.1016/j.celrep.2023.112289

SUMMARY

Myofibers are broadly characterized as fatigue-resistant slow-twitch (type I) fibers and rapidly fatiguing fast-twitch (type IIa/IIx/IIb) fibers. However, the molecular regulation of myofiber type is not entirely understood; particularly, information on regulators of fast-twitch muscle is scarce. Here, we demonstrate that the large Maf transcription factor family dictates fast type IIb myofiber specification in mice. Remarkably, the ablation of three large Mafs leads to the drastic loss of type IIb myofibers, resulting in enhanced endurance capacity and the reduction of muscle force. Conversely, the overexpression of each large Maf in the type I soleus muscle induces type IIb myofibers. Mechanistically, a large Maf directly binds to the Maf recognition element on the promoter of myosin heavy chain 4, which encodes the type IIb myosin heavy chain, driving its expression. This work identifies the large Maf transcription factor family as a major regulator for fast type IIb muscle determination.

INTRODUCTION

Skeletal muscles are composed of heterogeneous myofiber types. Specialized myofiber properties acquired at the end of fetal development and during the neonatal period remain plastic in response to contractile demand and various conditions, including exercise, immobilization, space flight, and aging. Myofibers can be broadly classified as slow-twitch (type I) and fast-twitch (type II) types. Slow type I myofibers are rich in mitochondria, exhibit high oxidative metabolism, and express slow isoforms of sarcomeric proteins, such as myosin heavy chain 7 (*Myh7*). Fast type II myofibers are subclassified as IIa, IIx, or IIb, depending on the expression of fast *Myh* isoforms (*Myh2, Myh1*, and *Myh4*). *Myh2*, *Myh1*, and *Myh4* encode myosin heavy chain (MyHC) IIa, IIx, and IIb, respectively. The proportion of each myofiber type can impact muscle function and metabolism, consequently influencing susceptibility to diabetes, muscular dystrophy, and sarcopenia.[1,2]

Aerobic exercise encourages a myofiber type transition toward a slower, more oxidative phenotype.[3] In contrast, prolonged inactivity, such as that which occurs during immobilization and microgravity in space, induces a slow-to-fast transition.[4,5] Researchers have begun to dissect the key factors and pathways driving the formation of slow oxidative myofibers.[6–10] Especially, the calcineurin-nuclear factor of activated T cells (NFAT) pathway, AMP-activated protein kinase (AMPK), and peroxisome proliferator-activated receptor gamma co-activator-1α (PGC-1α/Ppargc1a) form the center of the regulatory network that drives formation of slow oxidative myofibers.[7,11–14] However, less is known about transcription factors and signaling pathways relevant to distinct fast glycolytic myofiber gene determination.

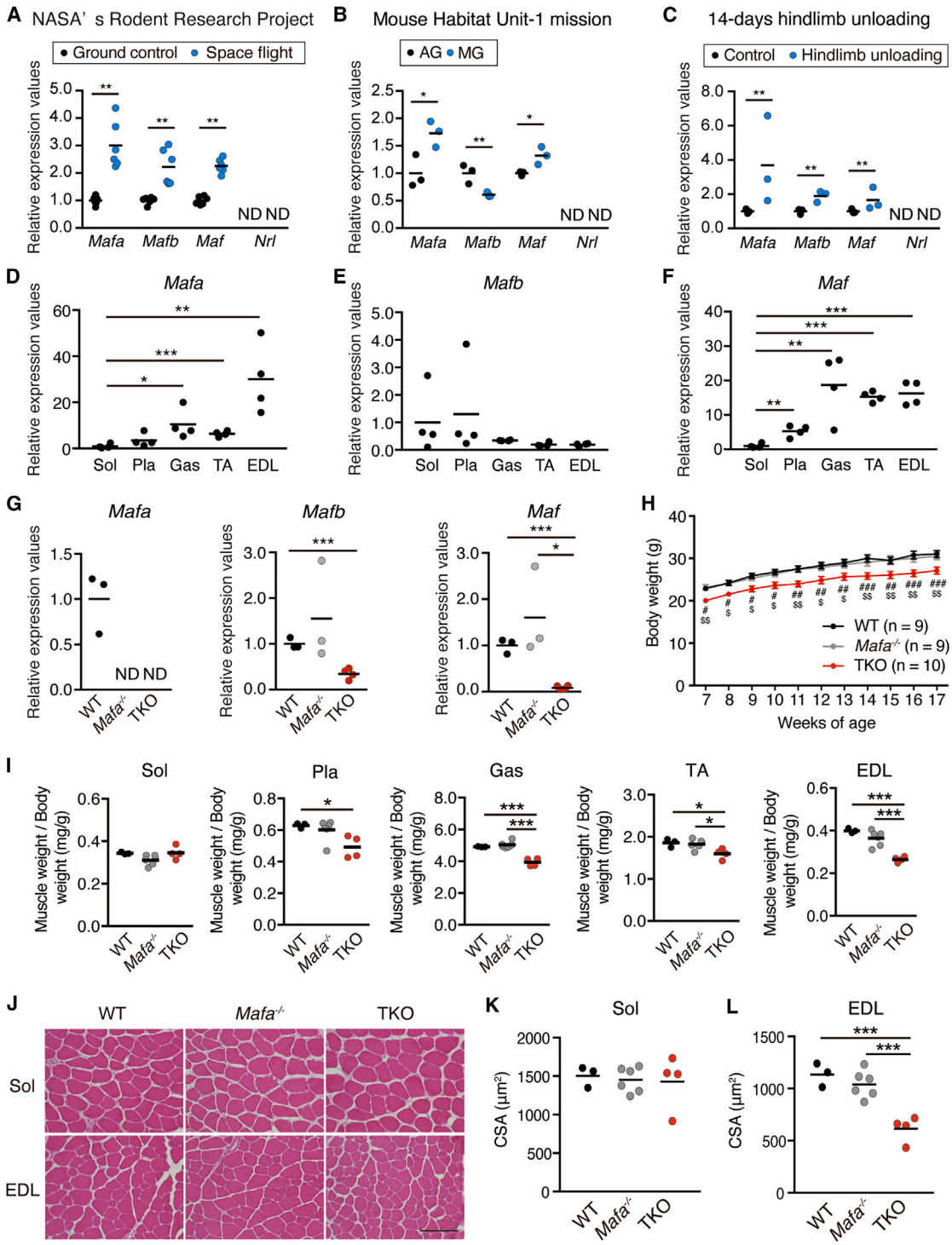

Figure 1. Large Mafs are enriched in fast glycolytic muscles and influence skeletal muscle morphology

(A) Relative mRNA levels of *Mafa*, *Mafb*, *Maf*, and *Nrl* in soleus muscles of mice after 37 days of space flight (extracted from GLDS-104 dataset, n = 6/group).

(B) Relative mRNA levels of *Mafa*, *Mafb*, *Maf*, and *Nrl* in soleus muscles after 31 days of space flight with different gravitational levels generated in the multiple artificial gravity system (MARS), as described in our previous report (DRA014336, n = 3/group).[4]

(C) Relative mRNA levels of *Mafa*, *Mafb*, and *Maf*, determined using qRT-PCR in soleus muscles following 14 day hindlimb unloading (n = 3/group).

(D–F) Relative mRNA levels of *Mafa* (D), *Mafb* (E), and *Maf* (F), determined using qRT-PCR in soleus (Sol), plantaris (Pla), gastrocnemius (Gas), tibialis anterior (TA), and extensor digitorum longus (EDL) muscles of 10-week-old male C57BL/6 mice (n = 4/group).

(legend continued on next page)

Some factors, such as Tbx15[15] and Sox6,[16–18] are associated with fast glycolytic myofiber. However, they function by repressing slow myofiber specification rather than by encouraging a fast glycolytic myofiber phenotype. The forced expression of Six1, a homeodomain-containing transcriptional factor, and its co-factor Eya1 in the soleus muscle of adult mice is sufficient to program a slow-to-fast myofiber transition in the presence of slow motoneuron innervation.[19] Six1 binds to the enhancer region of fast-twitch-specific genes (MEF3 site), including the common enhancers of *Myh1, Myh2,* and *Myh4*.[20–22] However, in a previous study, the conditional deletion of Six1 by human skeletal actin promoter led to a mere 20% reduction in *Myh4* transcripts, with an even slighter effect on the type IIb myofiber ratio in adult skeletal muscles.[21] Therefore, in addition to Six1 homeoproteins, another transcriptional factor must be required to regulate fast *Myh* expression. The discovery of such a transcriptional factor will inform new strategies for the prevention of unfavorable myofiber type transitions with aging and space travel.

We previously developed a multiple artificial gravity system (MARS) on the international space station (ISS), enabling us to study the effect of various gravitational loads on mammals.[23] Through whole-transcriptome analysis of skeletal muscles in mice exposed to microgravity or artificial gravity (1 *g*) in MARS,[4] we found that the expression of the large Maf transcription factor family responded dynamically to mechanical stimuli. In mammals, four large Mafs have been identified: Mafa, Mafb, Maf (c-Maf), and Nrl. These factors generally act as transcriptional activators via binding to Maf recognition elements (MAREs).[24,25] Large Mafs are expressed in a variety of cell types and play determinant roles in their development and differentiation, such as in pancreatic α and β cells,[26,27] macrophages,[28,29] and lens fiber cells.[30] Additionally, Mafb and Maf null mice exhibit embryonic lethality deriving from hindbrain abnormality, renal dysgenesis, respiratory failure, and impaired erythropoiesis in fetal liver.[31–34] Recently, single-nucleus assay for transposase-accessible chromatin sequencing (ATAC-seq) of skeletal muscle[35] revealed that NRL/Maf motifs are enriched in fast *Myh4* myonuclei, suggesting that large Mafs contribute to the activation of fast *Myh* gene in synergy with Six1. However, the role of large Mafs in adult skeletal muscle remains unknown.

These data led us to examine the potential roles of large Mafs in myofiber type determination. Through loss- and gain-of-function experiments *in vivo*, we show that large Mafs participate in triggering fast-twitch muscle gene programs, partly through direct binding to the MARE site upstream of *Myh4* in skeletal muscles. Deletion of three large Mafs in skeletal muscle leads to an almost complete loss of type IIb myofibers, resulting in increased endurance capacity and reduction of muscle force. Conversely, overexpression of large Maf proteins strongly induces type IIb myofibers in the soleus muscle, which normally contains few type IIb myofibers in adult mice. Collectively, our data identify large Mafs as robust transcriptional elements that directly regulate type IIb myofibers during development and adaptation of skeletal muscle.

RESULTS

Large Mafs are enriched in fast glycolytic muscles

We initially queried mRNA expression of large Mafs using a database from the NASA Rodent Research Project (GLDS-104) and confirmed that the expressions of *Mafa*, *Mafb*, and *Maf*, but not *Nrl*, were significantly upregulated in soleus muscles after space flight compared with their respective levels in ground control mice (Figure 1A). To further determine whether the upregulation of large Mafs was caused by disuse in space, and not by radiation or environmental stress during space flight, we reanalyzed the mRNA expression of large Mafs in soleus muscles exposed to different gravitational levels (microgravity [MG]; 1 *g* artificial gravity [AG]) in space using the MARS.[23] Consistent with Rodent Research Project findings, *Mafa* and *Maf* were significantly upregulated in MG mice when compared with levels in AG mice (Figure 1B). *Mafb* expression, on the other hand, was downregulated in MG compared with AG mice (Figure 1B). To examine the dynamics of large Mafs during muscle disuse, hindlimb unloading (HU), a model of MG, was performed. After 14 days of HU, the expression of *Mafa*, *Mafb*, and *Maf*, but not *Nrl*, in the soleus muscles was significantly higher in HU than in control mice (Figure 1C). These data suggest that three large Mafs, *Mafa*, *Mafb*, and *Maf*, were induced in the atrophied muscle with slow-to-fast myofiber transition.

Our qPCR analysis of various tissues of mice revealed that *Mafa* and *Maf* mRNA are predominantly enriched in the quadriceps muscles compared with those in other tissues (Figures S1A and S1C). *Mafb* showed its highest expression in the liver; however, quadriceps muscles also showed higher *Mafb* expression than other tissues such as the brain and the heart (Figure S1B). Assessment of individual muscles showed that the expression of *Mafa* and *Maf*, but not *Mafb*, was significantly higher in fast glycolytic muscles, such as the plantaris, gastrocnemius, tibialis anterior (TA), and extensor digitorum longus (EDL) muscles, than in the slow oxidative soleus muscle (Figures 1D–1F). Together, these data suggest that large Mafs were enriched in skeletal muscle, especially in fast glycolytic muscles.

Loss of large Mafs in skeletal muscle leads to a reduction in fast-twitch muscle mass

To characterize the role of large Mafs in skeletal muscle, we initially analyzed *Mafa, Mafb,* and *Maf* single knockout (KO)

(G) qPCR analysis for *Mafa*, *Mafb*, and *Maf* mRNA levels from the EDL of male TKO (n = 4), *Mafa*$^{-/-}$ (n = 3), and WT (n = 3) mice at 10–11 weeks of age.
(H) Body weight changes of male TKO, *Mafa*$^{-/-}$, and WT mice at 7 to 17 weeks of age (n = 9–10 mice per group).
(I) Skeletal muscle weights of male TKO (n = 4), *Mafa*$^{-/-}$ (n = 6), and WT (n = 3) mice at 10–11 weeks of age, normalized to body weight.
(J) Hematoxylin and eosin staining of Sol and EDL muscle cross-sections. Scale bar, 200 μm.
(K) Cross-sectional areas (CSAs) of Sol muscles of male TKO (n = 4), *Mafa*$^{-/-}$ (n = 6), and WT (n = 3) mice at 10–11 weeks of age.
(L) CSAs of EDL muscle of male TKO (n = 4), *Mafa*$^{-/-}$ (n = 6), and WT (n = 3) mice at 10–11 weeks of age.
p values were calculated using edgeR test (A–C), Student's t test (D–F), and Tukey's test (G–I, K, and L); *, #, or $p < 0.05, **, ##, or $$p < 0.01, ***, ###, or $$$p < 0.001, # TKO vs. WT, $ TKO vs. *Mafa*$^{-/-}$.

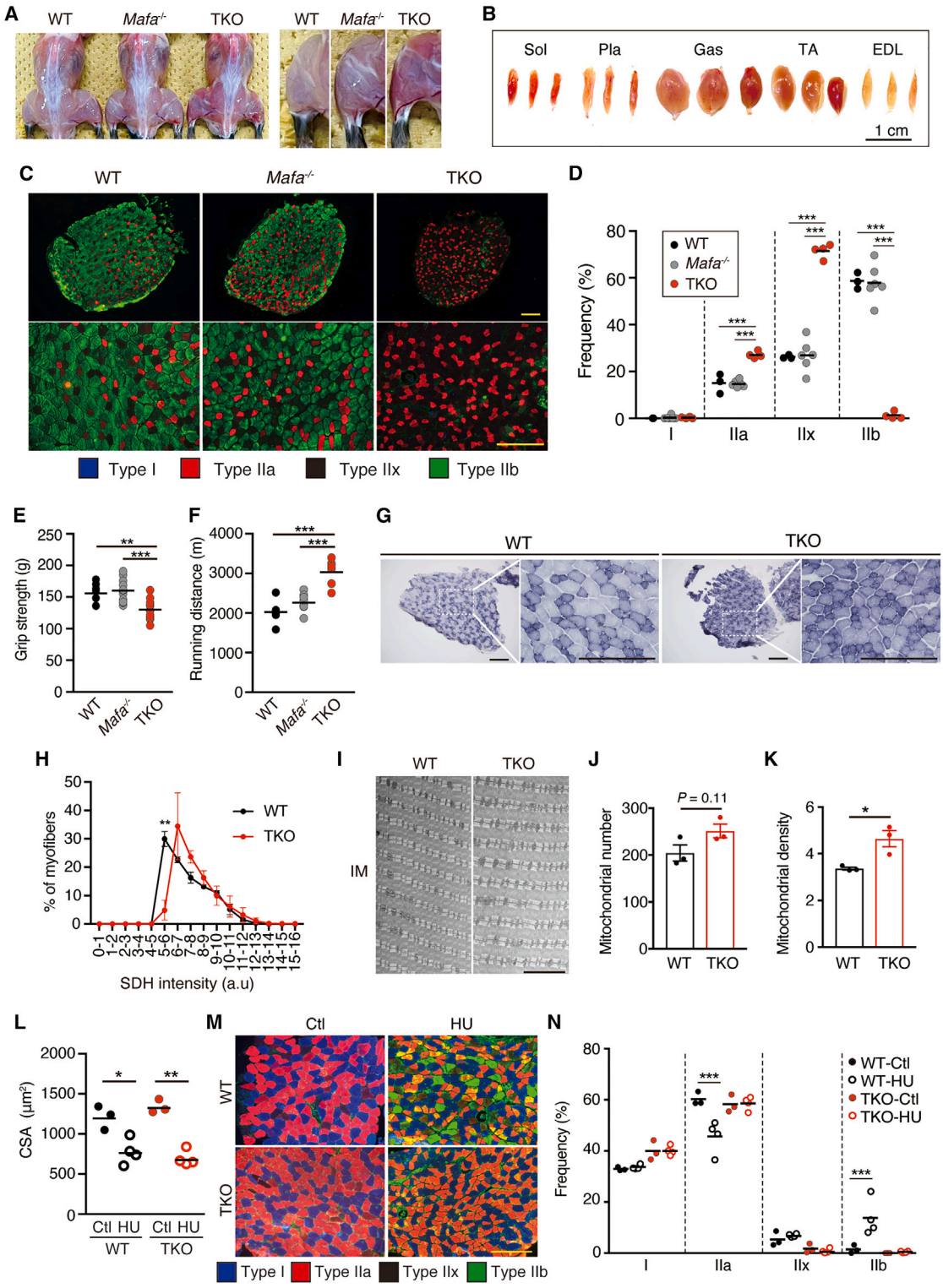

Figure 2. Large Maf depletion causes a dramatic loss of type IIb myofibers, reduced muscle force, and increased endurance capacity

(A) Dorsal view and dissected hindlimbs of TKO, *Mafa*$^{-/-}$, and WT mice at 10–11 weeks of age.

(B) Dissected individual hindlimb muscles of TKO, *Mafa*$^{-/-}$, and WT mice at 10–11 weeks of age.

(C) Immunostaining of the myosin heavy chain (MyHC) using myofiber-specific antibodies (type I, blue; type IIa, red; type IIb, green) on the EDL muscle. The unstained fibers are considered type IIx fibers (black). Scale bars, 200 μm.

(legend continued on next page)

mice. Single *Mafa* KO mice were indistinguishable from age-matched wild-type (WT) mice in terms of body weight (Figure 1H), muscle mass (Figure 1I), and myofiber size (Figures 1J–1L). Next, we analyzed the skeletal muscle-specific single *Mafb*- or *Maf*-deficient mice. *Mafb* or *Maf* floxed homozygous mice were crossed with HSA-Cre79 mice carrying Cre-recombinase expression under the control of the human α-skeletal actin (HSA) promoter,[36] resulting in conditional ablation of *Mafb* or Maf only in post-mitotic myofibers (*Mafb* conditional KO [cKO], *Maf* cKO) (Figures S2 and S3). We observed skeletal muscle-specific depletion of *Mafb* or Maf quantified by qPCR in adult mice (Figures S2A and S3A). As in *Mafa*-deficient mice, neither *Mafb* cKO nor *Maf* cKO mice exhibited drastic phenotypes of muscle weight, myofiber cross-sectional area (CSA), or myofiber type, with only a slightly reduced frequency of type IIx myofibers in *Mafb* cKO EDL muscles compared with that in WT mice (Figures S2B–S2G and S3B–S3G). Analysis of the skeletal muscle in *Mafb* and *Maf* double cKO (DKO) mice also showed no obvious signs of body weight or myofiber size changes compared with that in WT mice (Figures S4A–S4D).

Because *Mafa*, *Mafb*, and *Maf* bind to similar MARE sequences,[24,25] we hypothesized that large Mafs expressed in skeletal muscles can compensate for the function of each upon depletion of one or two of them (Figures 1G–1L, S2A–S2E, S3A–S3E, and S4A–S4D). To determine the roles of large Mafs in skeletal muscle, we established *Mafa*, *Mafb*, and *Maf* triple KO (TKO) mice by crossing $HSA^{Cre/+}$::$Mafb^{flox/flox}$::$Maf^{flox/flox}$ mice with a *Mafa*-deficient background and confirmed depletion of all large Mafs in the skeletal muscles of adult mice (Figure 1G). The body weight of TKO mice was slightly lower than that of WT and *Mafa* KO mice (Figure 1H). Muscle weight and histological examination showed a significant reduction of muscle mass and myofiber size in fast-twitch muscles (EDL, plantaris, gastrocnemius, and TA) of TKO mice compared with that in WT or *Mafa* KO mice (Figures 1I, 1J, and 1L). On the other hand, muscle weight and myofiber size in the slow-twitch soleus muscles were almost identical between TKO, WT, and *Mafa* KO mice (Figures 1I–1K). Major sex differences in these phenotypes were not observed, except for an increased size of the soleus muscle of female TKO mice (Figures S5A–S5C). Neither the abnormal structure of myofibers with central nucleation nor a reduction in number of myofibers, nor each type of myofiber size, was seen in any mouse (Figures 1J, S6A, and S6G). Despite the lack of major phenotype in skeletal muscle mass in single KO and DKO mice, ablation of three major large Mafs expressed in skeletal muscles significantly led to a significant reduction of fast-twitch muscle mass.

Loss of large Mafs in skeletal muscle leads to a complete loss of type IIb myofibers

We next analyzed myofiber types in TKO mice. From a gross morphological perspective, we observed that skeletal muscles from TKO mice were redder in appearance than those of WT and *Mafa* KO mice (Figures 2A and 2B). Immunohistochemical analysis using the MyHC I-, IIa-, and IIb-specific antibodies was performed to analyze the composition of myofiber types. The myofibers that were not stained with MyHC I, IIa, or IIb were classified as type IIx. Surprisingly, EDL muscle, which mainly comprises type IIb myofiber, exhibited an almost complete loss of type IIb myofibers along with a drastic increase in type IIx and a slight increase in type IIa myofibers in both male and female TKO mice (Figures 2C, 2D, S5E, and S6B). These observations were further confirmed using SDS-PAGE and qPCR for each MyHC isoform (Figures S7A–S7C and S7G). The drastic loss of type IIb myofibers was also observed in other fast-twitch muscles, including the plantaris, gastrocnemius, and TA (Figures S6D–S6F); however, no significant changes in the proportion of type IIb myofibers were detected in the soleus muscle of TKO mice (Figures S5D, S6C, and S7D–S7F). We also observed that *Mafb* and *Maf* DKO mice exhibited 10%–15% reduction of type IIb myofibers in the EDL muscles, but not in soleus muscles, compared with levels in WT mice (Figures S4E and S4F).

Next, we investigated how different myofiber type compositions affected muscle performance. Consistent with the loss of type IIb myofibers in TKO mice, average grip strength was significantly lower in TKO mice than in WT and *Mafa* KO mice (Figure 2E). We also measured time to exhaustion in a treadmill test. We observed that TKO mice ran longer than WT and *Mafa* KO mice (Figure 2F). Fast-to-slow myofiber type transition often affects the metabolic capacity of myofibers, including mitochondria biogenesis.[14] The EDL muscles of TKO mice demonstrated a significant increase in succinate dehydrogenase (SDH) activity relative to that in WT mice (Figures 2G and 2H). In the soleus

(D) Quantification of each myofiber type in the EDL muscles of male TKO (n = 4), $Mafa^{-/-}$ (n = 6), and WT (n = 3) mice at 10–11 weeks of age.
(E) Absolute muscle strength of male TKO (n = 7), $Mafa^{-/-}$ (n = 12), and WT (n = 11) mice at 9–10 weeks of age, measured by grip strength test.
(F) Endurance exercise capacity of TKO (n = 6), $Mafa^{-/-}$ (n = 9), and WT (n = 6) at 15–16 weeks of age, measured by a treadmill running test. Graph represents running distance (m).
(G) SDH staining in the EDL muscle of male TKO and WT mice at 10 weeks of age. Scale bars, 200 μm.
(H) Distribution of SDH intensity of the EDL muscle of male TKO and WT mice at 10 weeks of age (n = 3/group).
(I) Representative transmission electron micrographs of the EDL muscle of male TKO and WT mice at 16–17 weeks of age. Scale bars, 5 μm.
(J) Quantification of the number of mitochondria in EDL muscles of male TKO and WT mice at 16–17 weeks of age. 5–6 random images at 3,000× magnification were taken, and mitochondria were counted in a blinded fashion (n = 3/group).
(K) Quantification of mitochondrial density in EDL muscles of male TKO and WT mice at 16–17 weeks of age. 5–6 random images at 3,000× magnification were taken, and mitochondrial size were measured in a blinded fashion (n = 3/group).
(L) CSA of Sol muscle from male TKO and WT mice at 11 weeks of age after 14 day hindlimb unloading (HU; n = 4/group) and control conditions (Ctl; n = 3/group).
(M) Immunostaining of MyHC using myofiber type-specific antibodies (type I, blue; type IIa, red; type IIb, green) in the Sol muscles of male WT and TKO mice at 11 week of age after 14 days of HU. The unstained fibers were assumed to be type IIx fibers (black). Scale bars, 200 μm.
(N) Quantification of each myofiber type in the Sol muscles of male mice at 11 weeks of age from WT-Ctl (n = 3), WT-HU (n = 4), TKO-Ctl (n = 3), and TKO-HU (n = 4).
p values were calculated using Tukey's test (D–F) and Student's t test (H, J–L, and N); *p < 0.05, **p < 0.01, ***p < 0.001.

muscles, SDH activity was comparable between WT and TKO mice (Figures S6H and S6I). Additionally, there was a trend for increase in both number and density of mitochondria in the EDL muscles of TKO mice compared with that in WT mice (Figures 2I–2K). These results demonstrate that the ablation of large Mafs expressed in skeletal muscles induced a severe loss of type IIb myofiber, leading to a transition toward a type IIx-IIa myofiber phenotype, therefore influencing muscle performance.

To provide additional evidence that large Mafs are required for type IIb myofiber specification, we performed HU for 14 days by tail suspension, inducing marked atrophy and type IIb induction in slow-twitch soleus muscles. Although the degree of muscle atrophy after HU was similar in WT and TKO mice (Figure 2L), the induction of type IIb myofibers observed in WT mice after HU was completely abolished in TKO mice (Figures 2M and 2N). Collectively, these results indicate that large Mafs were essential for type IIb induction, but not muscle atrophy, during muscle development and adaptation.

Large Mafs regulate fast glycolytic gene programs through MARE sequences

To investigate whole gene expression profiles in the absence of large Mafs in skeletal muscles, we performed RNA sequencing of the EDL and soleus muscles from TKO and WT mice. Principal-component analysis (PCA) showed a distinct transcriptome distance between control and TKO mice regarding EDL muscles (Figure S8A). However, transcriptome distance between these groups in regard to the soleus muscle was shorter (Figure S8B). We observed robust transcriptional changes in TKO skeletal muscle, with 680 genes differentially regulated in the EDL muscle and 373 genes differentially regulated in the soleus muscle in relation to those in WT mice (Figure 3A). Induction of atrogene expression in TKO muscle was not observed (Figure S8C). Based on the immunohistochemical analysis (recall Figures 2C and 2D), the expression of most genes that are highly expressed in type IIb myofibers, including *Myh4* and *Actn3*, was significantly lower in TKO than in WT EDL muscle (Figure 3B). Conversely, genes that are highly expressed in other myofiber types (type I, IIa, and IIx), including *Myh7* (type I) and *Myh1* (type IIx), were significantly upregulated in TKO EDL muscle compared with those in WT muscles (Figure 3B). Analysis of genes associated with myofiber type transitions showed that myocyte enhancer factor 2C (*Mef2c*), which promotes slow oxidative myofibers,[6,8,37] was upregulated in TKO mice relative to those in WT mice (Figure 3C). However, other slow oxidative myofiber determination factors, including *Ppargc1a*,[11] were not altered in EDL TKO muscles when compared with levels in WT tissue. Furthermore, the transcriptional factors associated with fast glycolytic muscle genes, including *Six1*, *Six4*, *Tbx15*, *Fnip1*, *Eya1*, and *Smarcd3* (Baf60c),[15,19,20,38,39] were not obviously affected in TKO EDL muscle (Figure 3C). Moreover, the ablation of large Mafs mainly affected a series of glycolytic, but not oxidative, genes (Figure 3D), suggesting that large Mafs regulate fast-twitch and glycolysis-related gene programs.

Next, to identify the precise target of large Mafs in skeletal muscles, the genes with commonly altered expression in both EDL and soleus muscles of TKO mice were selected and analyzed for refinement of the target genes. Compared with respective levels in WT mice, 28 genes were upregulated and 22 were downregulated in both EDL and soleus muscles of TKO mice (Figure 3E). Gene Ontology (GO) analysis of 50 differentially expressed genes in TKO muscles revealed that 8 genes (*Actn3*, *Mybpc2*, *Myh4*, *Atp2a2*, *Myh7*, *Tnnc1*, *Tnni1*, and *Tnn1*) were related to the transition between fast- and slow-twitch myofiber and muscle contraction (Figures 3F and 3G). Because large Mafs generally act as transcription activators through MARE sequences,[29,30,40–42] we hypothesized that the downregulated genes (*Actn3*, *Mybpc2*, *Myh4*) in TKO muscles would be the direct target of these factors (Figure 3G). Furthermore, a drastic reduction of type IIb myofibers in TKO mice (Figures 2C, 2D, S7A–S7C, and S7G) led us to examine the direct interaction of large Mafs with the regulatory element of *Myh4*. We identified a potential MARE site 270 bp upstream of the transcription initiation site of *Myh4* that was highly conserved among multiple mammalian species according to the UCSC Genome Browser (Figure 3H). To determine whether Mafs bind to the MARE of *Myh4*, the putative Myh4 MARE region was ligated to a pGL4.10 vector to generate a luciferase-Myh4-MARE vector, and the plasmid was co-transfected with a Mafa, Mafb, or Maf expression vector into the HEK293T cell line. We generated an additional control reporter with a mutation in the Myh4 MARE sequence (luciferase-Myh4-ΔMARE) (Figure 3I). The luciferase activity of luciferase-Myh4-MARE was significantly upregulated in the presence of each large Maf. However, the luciferase-Myh4-ΔMARE showed a significant decrease in responsiveness to all three large Maf-expressing vectors compared with luciferase-Myh4 MARE (Figures 3J–3L). Interestingly, we observed no luciferase activity in luciferase-Myh1, -Myh2, and -Myh3 in the presence of any large Mafs, despite the existence of a putative MARE in Myh1 and Myh3 (Figures S9A–S9K). Taken together, these data suggest that large Mafs directly and specifically regulate type IIb myofiber genes, including *Myh4*, thorough their MARE sequences.

Large Mafs reprogram adult slow-twitch myofiber toward fast type IIb myofiber

To verify whether large Mafs directly regulate fast glycolytic muscle determination, we next overexpressed *Mafa*, *Mafb*, or *Maf* in the soleus muscles of WT mice using adeno-associated viral (AAV) vectors (AAV6) (Figures S10A, S10D, and S10G). We found that the proportion of type IIb myofibers, which were barely detected in adult soleus muscles, was significantly increased in all AAV-large Maf-treated soleus muscles when compared with that in saline-treated controls (Figures 4A, 4B, 4D, 4E, 4G, and 4H). We also observed dramatically increased levels of *Myh4* transcripts in all AAV-large Maf-treated soleus muscles (Figures 4C, 4F, and 4I). A positive correlation between the expression of each large *Maf* mRNA and the proportion of type IIb myofibers was confirmed (Figures S10B, S10E, and S10H). In addition to an increased level of *Myh4* expression, we found that glycolysis-related genes with MARE-like sequences, such as *Eno3*, *Ldha*, and *Tpi1*, were significantly upregulated in AAV-Mafb mice (Figure S10F). However, AAV-Mafa or AAV-Maf mice did not exhibit significantly induced expression of these genes, with a trend toward upregulation (Figures S10C

CellPress
OPEN ACCESS

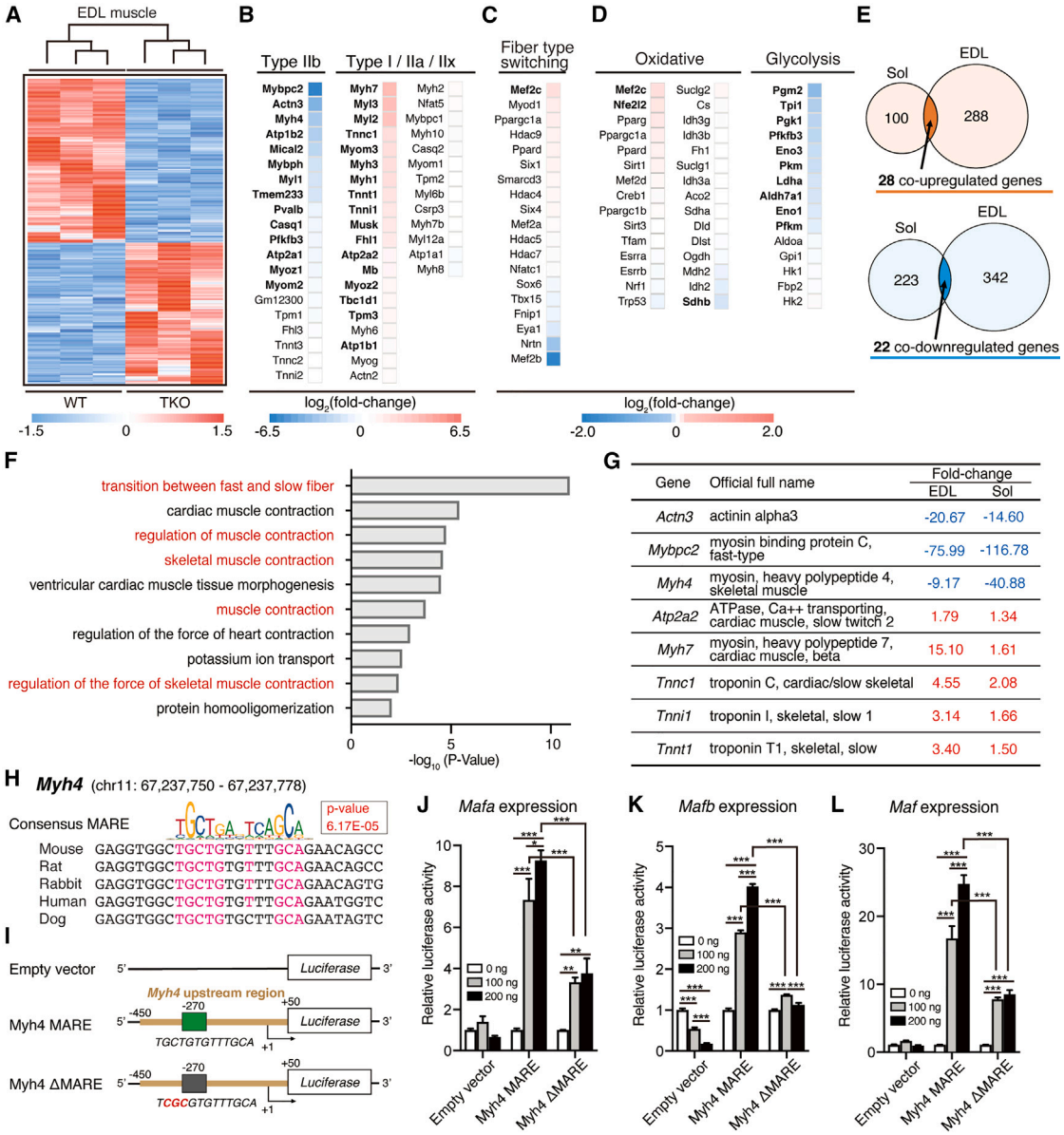

Gene	Official full name	Fold-change EDL	Fold-change Sol
Actn3	actinin alpha3	-20.67	-14.60
Mybpc2	myosin binding protein C, fast-type	-75.99	-116.78
Myh4	myosin, heavy polypeptide 4, skeletal muscle	-9.17	-40.88
Atp2a2	ATPase, Ca++ transporting, cardiac muscle, slow twitch 2	1.79	1.34
Myh7	myosin, heavy polypeptide 7, cardiac muscle, beta	15.10	1.61
Tnnc1	troponin C, cardiac/slow skeletal	4.55	2.08
Tnni1	troponin I, skeletal, slow 1	3.14	1.66
Tnnt1	troponin T1, skeletal, slow	3.40	1.50

Figure 3. The loss of large Mafs dramatically decreases fast glycolytic gene expression

(A) Heatmap visualizing differential gene expression in EDL muscles of male TKO and WT mice at 11 weeks of age (n = 3 mice per genotype).

(B) Heatmap visualizing expression of slow or fast type-specific genes in EDL muscles of male TKO and WT mice at 11 weeks of age (n = 3 mice per genotype).

(C) Heatmap visualizing expression of known myofiber type-regulating genes in EDL muscles of male TKO and WT mice at 11 weeks of age (n = 3 mice per genotype).

(D) Heatmap visualizing expression of mitochondria biogenesis-, TCA cycle-, and glycolysis-associated genes in EDL muscles of male TKO and WT mice at 11 weeks of age (n = 3 mice per genotype).

(E) Venn diagram showing the number of differentially expressed genes (DEGs) upregulated (top) and downregulated (bottom) in Sol and EDL muscles of TKO mice compared with those of WT mice.

(F) Gene Ontology (GO) analysis of genes up- or downregulated genes (50 total) in both Sol and EDL muscles in TKO.

(G) Gene list showing skeletal muscle contraction-related DEGs as shown in red in (F).

(H) MARE-like sequences in the promoter region of *Myh4* in mammalian species.

(I) Luciferase reporter constructs of *Myh4* upstream region (−450 to +50) containing a MARE-like (Myh4 MARE) or mutant MARE sequence (Myh4 ΔMARE).

(J–L) Relative Myh4-luciferase reporter activities in HEK293T cells overexpressing *Mafa* (J), *Mafb* (K), or *Maf* (L) (n = 3 per condition).

p values were calculated using Tukey's test (J–L); *p < 0.05, **p < 0.01, ***p < 0.001. Bold font (B–D) indicates statistical significance (edgeR test, p < 0.05).

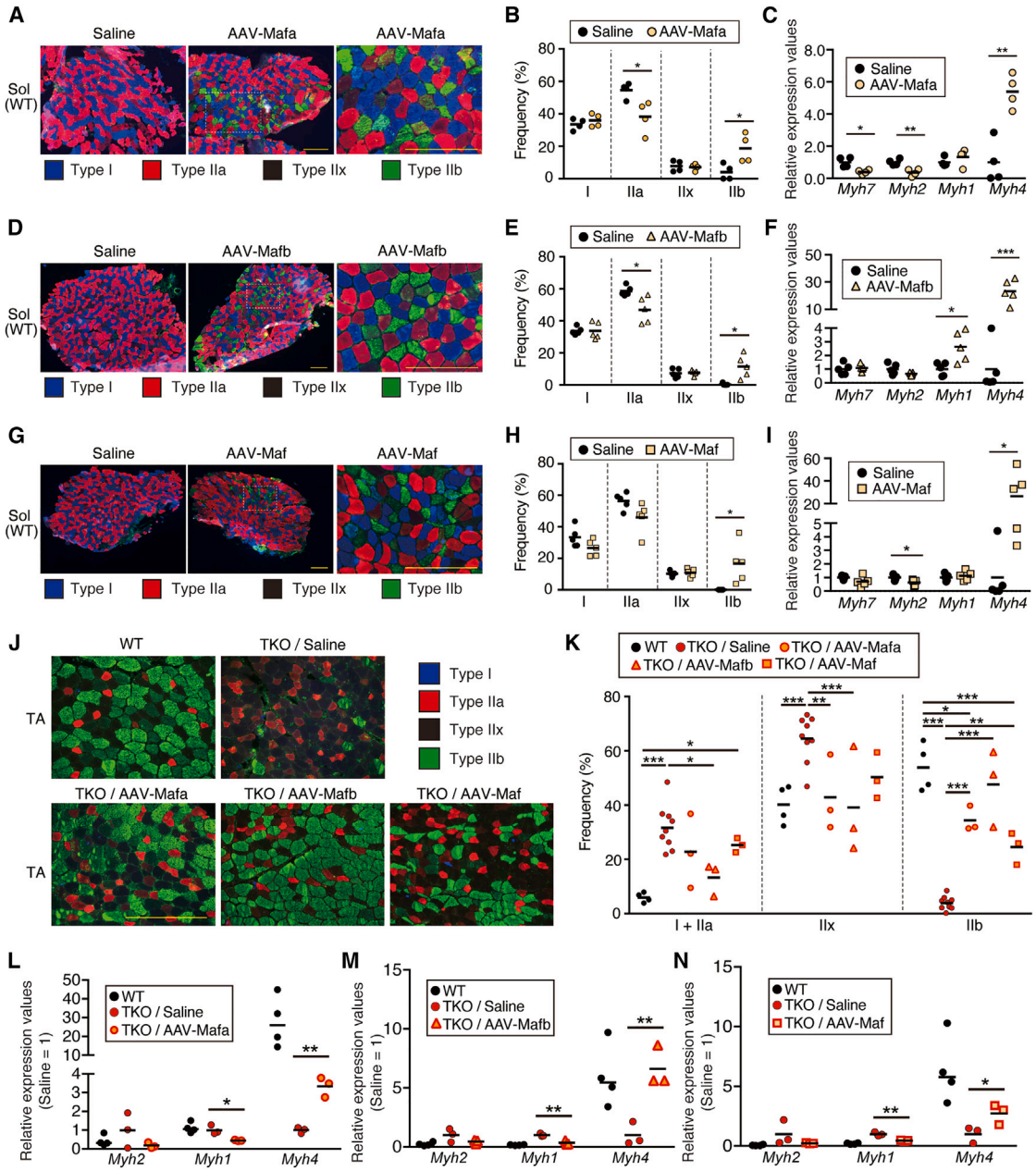

Figure 4. Overexpression of a large Maf favors type IIb myofibers

(A) Immunostaining of the MyHC using myofiber-specific antibodies (type I blue; type IIa, red; type IIb, green) in the Sol muscles of saline- or AAV-Mafa-treated WT mice. The unstained fibers are considered type IIx fibers (black). Scale bars, 200 μm.

(B) Frequency of each fiber type in the Sol muscles of saline- or AAV-Mafa-treated WT mice (n = 4/group).

(C) Relative mRNA levels of each *Myh*, determined using qRT-PCR in Sol muscles following saline or AAV-Mafa injection.

(D) Immunostaining of the MyHC using myofiber-specific antibodies (type I, blue; type IIa, red; type IIb, green) in the Sol muscles of saline- or AAV-Mafb-treated WT mice. The unstained fibers are considered type IIx fibers (black). Scale bars, 200 μm.

(E) Frequency of each fiber type in the Sol muscles of saline- or AAV-Mafb-treated WT mice (n = 5/group).

(F) Relative mRNA levels of each *Myh*, determined using qRT-PCR in Sol muscles following saline or AAV-Mafb injection.

(G) Immunostaining of MyHC using myofiber-specific antibodies (type I, blue; type IIa, red; type IIb, green) in the Sol muscles of saline- or AAV-Maf-treated WT mice. The unstained fibers are considered type IIx fibers (black). Scale bars, 200 μm.

(H) Frequency of each myofiber type in the Sol muscles of saline or AAV-Maf-treated WT mice (n = 5/group).

(I) Relative mRNA levels of each *Myh*, determined using qRT-PCR in Sol muscles following saline or AAV-Maf injection.

(J) Immunostaining of MyHC using myofiber-specific antibodies (type I, blue; type IIa, red; type IIb, green) in the TA muscles of male (n = 1) and female (n = 2) saline-, AAV-Mafa-, AAV-Mafb-, or AAV-Maf-treated TKO mice. Non-treated TA muscles of WT mice are also represented. Scale bars, 200 μm.

(legend continued on next page)

and S10I). These results collectively demonstrate that forced expression of a single large Maf in adult soleus muscles drives type IIb myofibers.

Finally, to test the hypothesis that a single large Maf directly drives the slow-to-fast myofiber transition, without the interaction of endogenous large Mafs, we overexpressed them in the TA muscles of TKO mice using the AAV-large Mafs vectors. We observed that the loss of type IIb myofiber in TA muscles of TKO mice was restored by all the AAV-large Mafs vectors, reflected by a significant increase in the proportion of type IIb myofibers (Figures 4J and 4K) and the strong upregulation of *Myh4*, *Actn3*, and *Mybpc2* expression (Figures 4L–4N and S10J–S10L). Results of our *in vivo* experiments together with *in vitro* luciferase assays indicate that large Mafs are able to reprogram type I, IIa, and IIx myofibers to fast IIb myofibers.

DISCUSSION

Since the discovery of the PGC-1α-PPARγ pathway as a central signal of slow oxidative myofiber determination, molecular mechanisms of slow oxidative myofiber formation have been extensively investigated.[11,12] In contrast, few robust transcriptional factors/pathways that regulate fast glycolytic myofiber formation have been identified. Using TKO alleles of all large Mafs expressed in skeletal muscles to avoid the compensatory mechanism of each large Maf, we showed almost complete loss of type IIb myofibers in hindlimb muscles of mice. Mechanistically, *in vitro* reporter assays and *in vivo* gene delivery experiments to manipulate large Maf expression in skeletal muscle revealed direct induction of fast type IIb myofiber gene programs, partly through MARE sequences. Interestingly, we did not detect any changes in *Six1*, *Six4*, *Smarcd3*, *Tbx15*, or *Fnip1* gene expression in TKO muscles, suggesting that large Mafs regulate fast type IIb muscle gene programs directly. To our knowledge, these findings represent the first evidence of a single transcriptional factor that specifically drives the fast type IIb myofibers.

Our RNA sequencing (RNA-seq) analysis of TKO muscle combined with *in vitro* reporter assays revealed that large Mafs specifically regulate the type IIb muscle gene *Myh4* through the MARE sequence. The other Myh isoforms (*Myh1*, *Myh2*, and *Myh3*) are not regulated by large Mafs. Furthermore, *in vivo* AAV-mediated overexpression of a single large Maf promoted not only *Myh4* expression but also other type IIb myofiber-specifically expressed genes, such as *Actn3* and *Mybpc2*. This suggests a degree of redundancy of Mafa, Mafb, and Maf in their ability to activate these genes. However, only Mafb promoted significant activation of glycolytic genes. Future study is warranted to elucidate the distinct roles of each large Maf in the determination of myofiber type.

Our data showed that slow-twitch muscle genes, including *Myh7*, which encodes type I myofibers, were upregulated in TKO muscles. However, the transcript levels of *Myh7* were significantly lower than those in soleus muscle of WT mice, making the actual protein undetectable in EDL muscles of TKO mice (Figures 2C, 2D, and S7A–S7C). The ablation of large Mafs did not induce the expression of slow oxidative myofiber specification genes such as *Hdac5/9*, *Nfatc1*, or *Ppargc1a* (PGC-1α). Only *Mef2c*, which regulates *Myh7*, was significantly increased in TKO muscles compared with that in WT muscles. Therefore, the contributions of large Mafs to direct regulation of slow-twitch muscle gene programs are likely minor.

SIX1 is major transcriptional factor that regulates fast Myh genes and fast-specific sarcomeric genes through the MEF3 site.[19–21,35] Recently, Dos Santos et al. identified a super enhancer at the fast Myh locus, associated with an active promotion of fast Myh genes.[22] Here, we identified a number of MARE-like sequences on the super enhancer element, including four MARE-like sequences in the enhancer region A, which is involved in the regulation of type IIb myofibers (Figures S11A and S11B). As SIX1 occupies the super-enhancer region by binding to the MEF3 site,[21,22] and since similar expression patterns are observed between large Mafs (Figure S12) and *Six1*[21] during muscle development, it is plausible that large Maf proteins are in close proximity to SIX1 proteins at the super-enhancer region through MARE-like sequences, thereby promoting the expression of fast Myh genes. Further study is required to scrutinize this interplay in the determination of myofiber type.

The present study identified that the large Maf family transcription factor is a major regulator for fast type IIb muscle formation. We are currently examining the long-term consequences of the ablation/overexpression of large Mafs in skeletal muscles on whole-body metabolism and lifespan. Additionally, identifying how the expression of the large Maf family transcriptional factor dynamically changes with aging will help in elucidating the molecular mechanisms by which the fast-to-slow myofiber transition occurs during aging in mammals, including humans.[2] However, whether preventing the fast-to-slow myofiber transition associated with aging could be a therapeutic option remains unclear, as the robust regulator inducing fast myofiber type in adult mice is limited. In the future, our discovery of large Mafs as a specific and robust regulator for type IIb myofiber determination will partly address this question of whether manipulating myofiber transition via overexpression or ablation of large Mafs can be a therapeutic option against age-related weakness of skeletal muscle. Moreover, given the potent role of the large Maf transcription factor family in the determination of fast type IIb myofibers, we anticipate that the manipulation of large Mafs, or of their regulators, may provide novel therapeutic interventions for the family of muscular dystrophies in which fast-to-slow transition protects the muscle from contraction-induced damage.[39,43,44]

(K) Frequency of each myofiber type in the TA muscles of WT mice (n = 4) and saline- (n = 9), AAV-Mafa- (n = 3), AAV-Mafb- (n = 3), or AAV-Maf-treated TKO mice (n = 3).

(L–N) Relative mRNA levels of each *Myh*, determined using qRT-PCR in TA muscles of WT (n = 4) and TKO (n = 3) following saline, AAV-Mafa (L), AAV-Mafb (M), or AAV-Maf (N) injection.

p values were calculated using Tukey's test (K) and Student's t test (B, C, E, F, H, I, and L–N); *p < 0.05, **p < 0.01, ***p < 0.001.

Limitation of the study

Our work used B6.Cg-Tg(ACTA1-cre)79Jme/J mice, in which gene deletions occur at the embryonic phase of muscle development; therefore, whether the large Maf family plays a functional role in the adult post-natal myofibers was remains to be addressed. Single-nucleus ATAC-seq of skeletal muscle[35] revealed that NRL/Maf motifs are enriched in fast *Myh4* myonuclei of adult mice; thus, further investigation using skeletal muscle-specific inducible Cre mice might reveal their potential role in the maintenance of type IIb myofibers in adult animals. The drastic transition of type IIb to type IIx/a myofibers in TKO mice results in enhanced mitochondrial activity and concomitant increased endurance. However, our RNA-seq analysis did not reveal significant changes of major mitochondrial-related genes. Only *Mef2c* and *Nfe2l2* (Nrf2) expression was significantly enhanced in the TKO muscles; hence, the precise molecular mechanism through which large Maf family factors regulate mitochondrial dynamics remains unanswered. We attempted to uncover the precise target of the large Maf family through analysis of genes altered in both EDL and soleus muscles of TKO compared with WT mice. Our current evidence supports the regulation of MARE-containing *Myh4*, *Actn3*, and *Mypbc2* (Figures S11C and S11D) by large Mafs; however, our screening strategy might have missed some genes targeted by the large Maf family. Furthermore, we show that large Mafs specifically regulated *Myh4* through MARE, but not *Myh1* or *Myh3*, where putative MARE-like sequences were also identified. As it appears that large Mafs bind favorably to the MARE on the *Myh4* promoter region, but not on that of *Myh1/3*, the extent to which the MARE sequence is required for large Maf binding remains unclear.

STAR★METHODS

Detailed methods are provided in the online version of this paper and include the following:

- KEY RESOURCES TABLE
- RESOURCE AVAILABILITY
  - Lead contact
  - Materials availability
  - Data and code availability
- EXPERIMENTAL MODELS AND SUBJECT DETAILS
  - Mice
- METHOD DETAILS
  - Data from GeneLab
  - RNA-seq analysis
  - Quantitative analysis of transcripts using reverse transcription PCR
  - SDS-PAGE
  - Histological analysis and immunohistochemistry of muscle cryosections
  - Grip strength test
  - Treadmill test
  - Transmission electron microscopy
  - Motif enrichment analysis
  - Luciferase assay
  - AAV-mediated skeletal muscle Mafa/Mafb/Maf overexpression
- QUANTIFICATION AND STATISTICAL ANALYSIS

SUPPLEMENTAL INFORMATION

Supplemental information can be found online at https://doi.org/10.1016/j.celrep.2023.112289.

ACKNOWLEDGMENTS

We would like to thank Dr. Iori Sakakibara (Aichi Medical University, Japan) for helpful discussions on the project. We also thank Dr. Fuminori Kawano (Matsumoto University) for providing the protocol for the SDS-PAGE of MyHC isoforms. This work was supported by the Grant-in-Aid for the Japan Aerospace Exploration Agency (14YPTK-005512; S. Takahashi); the Grant-in-Aid for Scientific Research on Innovative Area from MEXT (18H04965; S. Takahashi); the Japan Science and Technology Agency (JPMJPF2017; S. Takahashi); and the Ph.D. Program in Humanics (Doctoral Program for World-leading Innovative and Smart Education; S.S.). R.F. was funded by MEXT Leading Initiative for Excellent Young Researchers.

AUTHOR CONTRIBUTIONS

S.S., R.F., and S. Takahashi conceived the study and designed the experiments. S.S., T.H., A.N., Y.O., S.F., M.H., E.W., A.K., A.I., R.O., and D.S. performed the experiments. S.S., T.H., and M.M. performed RNA-seq analysis. S.S., R.F., T.K., S. Takeda, and S. Takahashi wrote the manuscript. All authors contributed to the analysis and interpretation of results and reviewed the manuscript.

DECLARATION OF INTERESTS

T.K., D.S., and S. Takahashi are inventors on a patent application related to this work (patent application no. 2022-083553).

Received: September 5, 2022
Revised: January 31, 2023
Accepted: March 6, 2023
Published: March 22, 2023

REFERENCES

1. Patti, M.E., Butte, A.J., Crunkhorn, S., Cusi, K., Berria, R., Kashyap, S., Miyazaki, Y., Kohane, I., Costello, M., Saccone, R., et al. (2003). Coordinated reduction of genes of oxidative metabolism in humans with insulin resistance and diabetes: potential role of *PGC1* and *NRF1*. Proc. Natl. Acad. Sci. USA *100*, 8466–8471. https://doi.org/10.1073/pnas.1032913100.
2. Schiaffino, S., and Reggiani, C. (2011). Fiber types in mammalian skeletal muscles. Physiol. Rev. *91*, 1447–1531. https://doi.org/10.1152/physrev.00031.2010.
3. Allen, D.L., Harrison, B.C., Maass, A., Bell, M.L., Byrnes, W.C., and Leinwand, L.A. (2001). Cardiac and skeletal muscle adaptations to voluntary wheel running in the mouse. J. Appl. Physiol. *90*, 1900–1908. https://doi.org/10.1152/jappl.2001.90.5.1900.
4. Okada, R., Fujita, S.I., Suzuki, R., Hayashi, T., Tsubouchi, H., Kato, C., Sadaki, S., Kanai, M., Fuseya, S., Inoue, Y., et al. (2021). Transcriptome analysis of gravitational effects on mouse skeletal muscles under microgravity and artificial 1 g onboard environment. Sci. Rep. *11*, 9168. https://doi.org/10.1038/s41598-021-88392-4.
5. Hayashi, T., Kudo, T., Fujita, R., Fujita, S.I., Tsubouchi, H., Fuseya, S., Suzuki, R., Hamada, M., Okada, R., Muratani, M., et al. (2021). Nuclear factor E2-related factor 2 (NRF2) deficiency accelerates fast fibre type transition in soleus muscle during space flight. Commun. Biol. *4*, 787. https://doi.org/10.1038/s42003-021-02334-4.

6. Wu, H., Naya, F.J., McKinsey, T.A., Mercer, B., Shelton, J.M., Chin, E.R., Simard, A.R., Michel, R.N., Bassel-Duby, R., Olson, E.N., and Williams, R.S. (2000). MEF2 responds to multiple calcium-regulated signals in the control of skeletal muscle fiber type. EMBO J. *19*, 1963–1973. https://doi.org/10.1093/emboj/19.9.1963.

7. Serrano, A.L., Murgia, M., Pallafacchina, G., Calabria, E., Coniglio, P., Lømo, T., and Schiaffino, S. (2001). Calcineurin controls nerve activity-dependent specification of slow skeletal muscle fibers but not muscle growth. Proc. Natl. Acad. Sci. USA *98*, 13108–13113. https://doi.org/10.1073/pnas.231148598.

8. Potthoff, M.J., Wu, H., Arnold, M.A., Shelton, J.M., Backs, J., McAnally, J., Richardson, J.A., Bassel-Duby, R., and Olson, E.N. (2007). Histone deacetylase degradation andMEF2 activation promote the formation of slow-twitch myofibers. J. Clin. Invest. *117*, 2459–2467. https://doi.org/10.1172/JCI31960.

9. Calabria, E., Ciciliot, S., Moretti, I., Garcia, M., Picard, A., Dyar, K.A., Pallafacchina, G., Tothova, J., Schiaffino, S., and Murgia, M. (2009). NFAT isoforms control activity-dependent muscle fiber type specification. Proc. Natl. Acad. Sci. USA *106*, 13335–13340. https://doi.org/10.1073/pnas.0812911106.

10. Ehlers, M.L., Celona, B., and Black, B.L. (2014). NFATc1 controls skeletal muscle fiber type and is a negative regulator of MyoD activity. Cell Rep. *8*, 1639–1648. https://doi.org/10.1016/j.celrep.2014.08.035.

11. Lin, J., Wu, H., Tarr, P.T., Zhang, C.-Y., Wu, Z., Boss, O., Michael, L.F., Puigserver, P., Isotani, E., Olson, E.N., et al. (2002). Transcriptional co-activator PGC-1α drives the formation of slow-twitch muscle fibres. Nature *418*, 797–801. https://doi.org/10.1038/nature00904.

12. Schuler, M., Ali, F., Chambon, C., Duteil, D., Bornert, J.-M., Tardivel, A., Desvergne, B., Wahli, W., Chambon, P., and Metzger, D. (2006). PGC1α expression is controlled in skeletal muscles by PPARβ, whose ablation results in fiber-type switching, obesity, and type 2 diabetes. Cell Metab. *4*, 407–414. https://doi.org/10.1016/j.cmet.2006.10.003.

13. Zechner, C., Lai, L., Zechner, J.F., Geng, T., Yan, Z., Rumsey, J.W., Collia, D., Chen, Z., Wozniak, D.F., Leone, T.C., and Kelly, D.P. (2010). Total skeletal muscle PGC-1 deficiency uncouples mitochondrial derangements from fiber type determination and insulin sensitivity. Cell Metab. *12*, 633–642. https://doi.org/10.1016/j.cmet.2010.11.008.

14. Correia, J.C., Kelahmetoglu, Y., Jannig, P.R., Schweingruber, C., Shvaikovskaya, D., Zhengye, L., Cervenka, I., Khan, N., Stec, M., Oliveira, M., et al. (2021). Muscle-secreted neurturin couples myofiber oxidative metabolism and slow motor neuron identity. Cell Metab. *33*, 2215–2230.e8. https://doi.org/10.1016/j.cmet.2021.09.003.

15. Lee, K.Y., Singh, M.K., Ussar, S., Wetzel, P., Hirshman, M.F., Goodyear, L.J., Kispert, A., and Kahn, C.R. (2015). Tbx15 controls skeletal muscle fibre-type determination and muscle metabolism. Nat. Commun. *6*, 8054. https://doi.org/10.1038/ncomms9054.

16. Hagiwara, N., Ma, B., and Ly, A. (2005). Slow and fast fiber isoform gene expression is systematically altered in skeletal muscle of the Sox6 mutant,p100H. Dev. Dyn. *234*, 301–311. https://doi.org/10.1002/dvdy.20535.

17. van Rooij, E., Quiat, D., Johnson, B.A., Sutherland, L.B., Qi, X., Richardson, J.A., Kelm, R.J., and Olson, E.N. (2009). A family of microRNAs encoded by myosin genes governs myosin expression and muscle performance. Dev. Cell *17*, 662–673. https://doi.org/10.1016/j.devcel.2009.10.013.

18. Quiat, D., Voelker, K.A., Pei, J., Grishin, N.V., Grange, R.W., Bassel-Duby, R., and Olson, E.N. (2011). Concerted regulation of myofiber-specific gene expression and muscle performance by the transcriptional repressor Sox6. Proc. Natl. Acad. Sci. USA *108*, 10196–10201. https://doi.org/10.1073/pnas.1107413108.

19. Grifone, R., Laclef, C., Spitz, F., Lopez, S., Demignon, J., Guidotti, J.-E., Kawakami, K., Xu, P.-X., Kelly, R., Petrof, B.J., et al. (2004). Six1 and Eya1 expression can reprogram adult muscle from the slow-twitch phenotype into the fast-twitch phenotype. Mol. Cell Biol. *24*, 6253–6267. https://doi.org/10.1128/MCB.24.14.6253-6267.2004.

20. Niro, C., Demignon, J., Vincent, S., Liu, Y., Giordani, J., Sgarioto, N., Favier, M., Guillet-Deniau, I., Blais, A., and Maire, P. (2010). Six1 and Six4 gene expression is necessary to activate the fast-type muscle gene program in the mouse primary myotome. Dev. Biol. *338*, 168–182. https://doi.org/10.1016/j.ydbio.2009.11.031.

21. Sakakibara, I., Santolini, M., Ferry, A., Hakim, V., and Maire, P. (2014). Six homeoproteins and a linc-RNA at the fast MYH locus lock fast myofiber terminal phenotype. PLoS Genet. *10*, e1004386. https://doi.org/10.1371/journal.pgen.1004386.

22. Dos Santos, M., Backer, S., Auradé, F., Wong, M.M.-K., Wurmser, M., Pierre, R., Langa, F., Do Cruzeiro, M., Schmitt, A., Concordet, J.-P., et al. (2022). A fast Myosin super enhancer dictates muscle fiber phenotype through competitive interactions with Myosin genes. Nat. Commun. *13*, 1039. https://doi.org/10.1038/s41467-022-28666-1.

23. Shiba, D., Mizuno, H., Yumoto, A., Shimomura, M., Kobayashi, H., Morita, H., Shimbo, M., Hamada, M., Kudo, T., Shinohara, M., et al. (2017). Development of new experimental platform 'MARS'—multiple Artificial-gravity Research System—to elucidate the impacts of micro/partial gravity on mice. Sci. Rep. *7*, 10837. https://doi.org/10.1038/s41598-017-10998-4.

24. Kataoka, K., Noda, M., and Nishizawa, M. (1994). Maf nuclear oncoprotein recognizes sequences related to an AP-1 site and forms heterodimers with both Fos and Jun. Mol. Cell Biol. *14*, 700–712. https://doi.org/10.1128/mcb.14.1.700-712.1994.

25. Yoshida, T., Ohkumo, T., Ishibashi, S., and Yasuda, K. (2005). The 5'-AT-rich half-site of Maf recognition element: a functional target for bZIP transcription factor Maf. Nucleic Acids Res. *33*, 3465–3478. https://doi.org/10.1093/nar/gki653.

26. Artner, I., Blanchi, B., Raum, J.C., Guo, M., Kaneko, T., Cordes, S., Sieweke, M., and Stein, R. (2007). MafB is required for islet beta cell maturation. Proc. Natl. Acad. Sci. USA *104*, 3853–3858. https://doi.org/10.1073/pnas.0700013104.

27. Zhang, C., Moriguchi, T., Kajihara, M., Esaki, R., Harada, A., Shimohata, H., Oishi, H., Hamada, M., Morito, N., Hasegawa, K., et al. (2005). MafA is a key regulator of glucose-stimulated insulin secretion. Mol. Cell Biol. *25*, 4969–4976. https://doi.org/10.1128/MCB.25.12.4969-4976.2005.

28. Hamada, M., Tsunakawa, Y., Jeon, H., Yadav, M.K., and Takahashi, S. (2020). Role of MafB in macrophages. Exp. Anim. *69*, 1–10. https://doi.org/10.1538/expanim.19-0076.

29. Hamada, M., Nakamura, M., Tran, M.T.N., Moriguchi, T., Hong, C., Ohsumi, T., Dinh, T.T.H., Kusakabe, M., Hattori, M., Katsumata, T., et al. (2014). MafB promotes atherosclerosis by inhibiting foam-cell apoptosis. Nat. Commun. *5*, 3147. https://doi.org/10.1038/ncomms4147.

30. Kawauchi, S., Takahashi, S., Nakajima, O., Ogino, H., Morita, M., Nishizawa, M., Yasuda, K., and Yamamoto, M. (1999). Regulation of lens fiber cell differentiation by transcription factor c-Maf. J. Biol. Chem. *274*, 19254–19260. https://doi.org/10.1074/jbc.274.27.19254.

31. Blanchi, B., Kelly, L.M., Viemari, J.-C., Lafon, I., Burnet, H., Bévengut, M., Tillmanns, S., Daniel, L., Graf, T., Hilaire, G., and Sieweke, M.H. (2003). MafB deficiency causes defective respiratory rhythmogenesis and fatal central apnea at birth. Nat. Neurosci. *6*, 1091–1100. https://doi.org/10.1038/nn1129.

32. Cordes, S.P., and Barsh, G.S. (1994). The mouse segmentation gene kr encodes a novel basic domain-leucine zipper transcription factor. Cell *79*, 1025–1034. https://doi.org/10.1016/0092-8674(94)90033-7.

33. Kusakabe, M., Hasegawa, K., Hamada, M., Nakamura, M., Ohsumi, T., Suzuki, H., Tran, M.T.N., Kudo, T., Uchida, K., Ninomiya, H., et al. (2011). c-Maf plays a crucial role for the definitive erythropoiesis that accompanies erythroblastic island formation in the fetal liver. Blood *118*, 1374–1385. https://doi.org/10.1182/blood-2010-08-300400.

34. Moriguchi, T., Hamada, M., Morito, N., Terunuma, T., Hasegawa, K., Zhang, C., Yokomizo, T., Esaki, R., Kuroda, E., Yoh, K., et al. (2006). MafB is essential for renal development and F4/80 expression in macrophages. Mol. Cell Biol. *26*, 5715–5727. https://doi.org/10.1128/MCB.00001-06.

35. Dos Santos, M., Backer, S., Saintpierre, B., Izac, B., Andrieu, M., Letournel, F., Relaix, F., Sotiropoulos, A., and Maire, P. (2020). Single-nucleus RNA-seq and FISH identify coordinated transcriptional activity in mammalian myofibers. Nat. Commun. *11*, 5102. https://doi.org/10.1038/s41467-020-18789-8.

36. Miniou, P., Tiziano, D., Frugier, T., Roblot, N., Le Meur, M., and Melki, J. (1999). Gene targeting restricted to mouse striated muscle lineage. Nucleic Acids Res. *27*, e27. https://doi.org/10.1093/nar/27.19.e27.

37. Chin, E.R., Olson, E.N., Richardson, J.A., Yang, Q., Humphries, C., Shelton, J.M., Wu, H., Zhu, W., Bassel-Duby, R., and Williams, R.S. (1998). A calcineurin-dependent transcriptional pathway controls skeletal muscle fiber type. Genes Dev. *12*, 2499–2509. https://doi.org/10.1101/gad.12.16.2499.

38. Meng, Z.-X., Li, S., Wang, L., Ko, H.J., Lee, Y., Jung, D.Y., Okutsu, M., Yan, Z., Kim, J.K., and Lin, J.D. (2013). Baf60c drives glycolytic metabolism in the muscle and improves systemic glucose homeostasis through Deptor-mediated Akt activation. Nat. Med. *19*, 640–645. https://doi.org/10.1038/nm.3144.

39. Reyes, N.L., Banks, G.B., Tsang, M., Margineantu, D., Gu, H., Djukovic, D., Chan, J., Torres, M., Liggitt, H.D., Hirenallur-S, D.K., et al. (2015). Fnip1 regulates skeletal muscle fiber type specification, fatigue resistance, and susceptibility to muscular dystrophy. Proc. Natl. Acad. Sci. USA *112*, 424–429. https://doi.org/10.1073/pnas.1413021112.

40. Tran, M.T.N., Hamada, M., Jeon, H., Shiraishi, R., Asano, K., Hattori, M., Nakamura, M., Imamura, Y., Tsunakawa, Y., Fujii, R., et al. (2017). MafB is a critical regulator of complement component C1q. Nat. Commun. *8*, 1700. https://doi.org/10.1038/s41467-017-01711-0.

41. Usui, T., Morito, N., Shawki, H.H., Sato, Y., Tsukaguchi, H., Hamada, M., Jeon, H., Yadav, M.K., Kuno, A., Tsunakawa, Y., et al. (2020). Transcription factor MafB in podocytes protects against the development of focal segmental glomerulosclerosis. Kidney Int. *98*, 391–403. https://doi.org/10.1016/j.kint.2020.02.038.

42. Nishikawa, K., Nakashima, T., Takeda, S., Isogai, M., Hamada, M., Kimura, A., Kodama, T., Yamaguchi, A., Owen, M.J., Takahashi, S., and Takayanagi, H. (2010). Maf promotes osteoblast differentiation in mice by mediating the age-related switch in mesenchymal cell differentiation. J. Clin. Invest. *120*, 3455–3465. https://doi.org/10.1172/JCI42528.

43. Selsby, J.T., Morine, K.J., Pendrak, K., Barton, E.R., and Sweeney, H.L. (2012). Rescue of dystrophic skeletal muscle by PGC-1α involves a fast to slow fiber type shift in the mdx mouse. PLoS One *7*, e30063. https://doi.org/10.1371/journal.pone.0030063.

44. Babaeijandaghi, F., Cheng, R., Kajabadi, N., Soliman, H., Chang, C.-K., Smandych, J., Tung, L.W., Long, R., Ghassemi, A., and Rossi, F.M.V. (2022). Metabolic reprogramming of skeletal muscle by resident macrophages points to CSF1R inhibitors as muscular dystrophy therapeutics. Sci. Transl. Med. *14*, eabg7504. https://doi.org/10.1126/scitranslmed.abg7504.

45. Tran, M.T.N., Hamada, M., Nakamura, M., Jeon, H., Kamei, R., Tsunakawa, Y., Kulathunga, K., Lin, Y.Y., Fujisawa, K., Kudo, T., and Takahashi, S. (2016). MafB deficiency accelerates the development of obesity in mice. FEBS Open Bio *6*, 540–547. https://doi.org/10.1002/2211-5463.12058.

46. Fujino, M., Tagami, A., Ojima, M., Mizuno, S., Abdellatif, A.M., Kuno, A., and Takahashi, S. (2020). c-MAF deletion in adult C57BL/6J mice induces cataract formation and abnormal differentiation of lens fiber cells. Exp. Anim. *69*, 242–249. https://doi.org/10.1538/expanim.19-0137.

47. Huang, D.W., Sherman, B.T., and Lempicki, R.A. (2009). Systematic and integrative analysis of large gene lists using DAVID bioinformatics resources. Nat. Protoc. *4*, 44–57. https://doi.org/10.1038/nprot.2008.211.

48. Kawano, F., Fujita, R., Nakai, N., Terada, M., Ohira, T., and Ohira, Y. (2012). HSP25 can modulate myofibrillar desmin cytoskeleton following the phosphorylation at Ser15 in rat soleus muscle. J. Appl. Physiol. *112*, 176–186. https://doi.org/10.1152/japplphysiol.00783.2011.

49. Satow, A., Maehara, S., Ise, S., Hikichi, H., Fukushima, M., Suzuki, G., Kimura, T., Tanak, T., Ito, S., Kawamoto, H., and Ohta, H. (2008). Pharmacological effects of the metabotropic glutamate receptor 1 antagonist compared with those of the metabotropic glutamate receptor 5 antagonist and metabotropic glutamate receptor 2/3 agonist in rodents: detailed investigations with a selective allosteric metabotropic glutamate receptor 1 antagonist, FTIDC [4-[1-(2-Fluoropyridine-3-yl)-5-methyl-1 *H* -1,2,3-triazol-4-yl]- *N* -isopropyl- *N* -methyl-3,6-dihydropyridine-1(2 *H*)-carboxamide]. J. Pharmacol. Exp. Ther. *326*, 577–586. https://doi.org/10.1124/jpet.108.138107.

50. Fujita, R., Yoshioka, K., Seko, D., Suematsu, T., Mitsuhashi, S., Senoo, N., Miura, S., Nishino, I., and Ono, Y. (2018). Zmynd17 controls muscle mitochondrial quality and whole-body metabolism. FASEB J. *32*, 5012–5025. https://doi.org/10.1096/fj.201701264R.

51. Grant, C.E., Bailey, T.L., and Noble, W.S. (2011). FIMO: scanning for occurrences of a given motif. Bioinformatics *27*, 1017–1018. https://doi.org/10.1093/bioinformatics/btr064.

STAR★METHODS

KEY RESOURCES TABLE

REAGENT or RESOURCE	SOURCE	IDENTIFIER
Antibodies		
mouse anti-MyHC type I	DSHB	Cat# BA-D5; RRID: AB_2235587
mouse anti-MyHC type IIa	DSHB	Cat# SC-71; RRID: AB_2147165
mouse anti-MyHC type IIx	DSHB	Cat# 6H1; RRID: AB_2314830
mouse anti-MyHC type IIb	DSHB	Cat# BF-F3; RRID: AB_2266724
Goat anti-Mouse IgG2b Cross-Adsorbed Secondary Antibody, Alexa Fluor™ 350	Thermo-Fisher Scientific	Cat# A-21140; RRID: AB_2535777
Goat anti-Mouse IgG1 Cross-Adsorbed Secondary Antibody, Alexa Fluor™ 555	Thermo-Fisher Scientific	Cat# A-21127; RRID: AB_2535769
Goat anti-Mouse IgM (Heavy chain) Cross-Adsorbed Secondary Antibody, Alexa Fluor™ 488	Thermo-Fisher Scientific	Cat# A-21042; RRID: AB_2535711
Bacterial and virus strains		
AAV6-CMV-Flag-Mafa	This study	N/A
AAV6-CMV-Flag-Mafb	This study	N/A
AAV6-CMV-Flag-Maf	This study	N/A
Chemicals, peptides, and recombinant proteins		
TRIzol	Thermo-Fisher Scientific	Cat# 15596026
ISOGEN	NIPPON GENE	Cat# 311-02501
Chloroform	FUJIFILM Wako Pure Chemical Corporation	Cat# 038-02606
Isopropanol	FUJIFILM Wako Pure Chemical Corporation	Cat# 166-04836
THUNDERBIRD® SYBR®qPCR Mix	TOYOBO	Cat# QPS-201
Isopentan	FUJIFILM Wako Pure Chemical Corporation	Cat# 168-09195
M.O.M. blocking reagent	Vector Laboratories	Cat# BMK-2202
Vibrance Antifade Mounting Medium	VECTASHIELD	Cat# H-1700
FuGENE® HD Transfection Reagent	Promega	Cat# E2311
In-Fusion Cloning HD Kit	Takara Bio	Cat# 639648
PrimeSTAR®GXL DNA Polymerase	Takara Bio	Cat# R050A
AAVpro®Helper Free System (AAV6)	Takara Bio	Cat# 6651
AAVpro Purification Kit	Takara Bio	Cat# 6666
AAVpro® Titration Kit (for real-time PCR) Ver.2	Takara Bio	Cat# 6233
Bio-Safe CBB G-250 Stain	BIO-RAD	Cat# 1610786
L-Glutamine	Gibco™	Cat# 25030081
Penicillin-Streptomycin	Gibco™	Cat# 15140122
MEM non-essential amino acid	Gibco™	Cat# 11140050
Sodium Pyruvate	Gibco™	Cat# 11360070
DMEM, high glucose, no glutamine	Gibco™	Cat# 11960044
DPBS, no calcium, no magnesium	Gibco™	Cat# 14190144
Fetal Bovine Serum, qualified, Brazil	Gibco™	Cat# 10270106
di-Sodium succinate hexahydrate	Kanto Chemical Co., Inc.	Cat# 37276-30
Nitro Blue Tetrazolium Chloride	FUJIFILM Wako Pure Chemical Corporation	Cat# 144-01993
Glycerol Gelatin	Sigma-Aldrich	Cat# GG1-15ML

(*Continued on next page*)

Continued

REAGENT or RESOURCE	SOURCE	IDENTIFIER
Acrylamide	FUJIFILM Wako Pure Chemical Corporation	Cat# 011-08015
N,N′-Methylenebis(acrylamide)	FUJIFILM Wako Pure Chemical Corporation	Cat# 138-06032
Glycerol	FUJIFILM Wako Pure Chemical Corporation	Cat# 075-00616
Mayer's Hematoxylin Solution	FUJIFILM Wako Pure Chemical Corporation	Cat# 131-09665
Goat Serum, New Zealand origin	Gibco™	Cat# 16210064
Bovine Serum Albumin	Sigma-Aldrich	Cat# A7906
Tragacanth Gum, Powder	FUJIFILM Wako Pure Chemical Corporation	Cat# 200-02245
DPX. Neutral mounting medium	Sigma-Aldrich	Cat# 317616
RNase-free Water, non DEPC	Biodynamics Laboratory Inc.	Cat# DR127
Ethanol (99.5)	FUJIFILM Wako Pure Chemical Corporation	Cat# 057-00456
Ethanol (99)	FUJIFILM Wako Pure Chemical Corporation	Cat# 056-06967
Xylene	FUJIFILM Wako Pure Chemical Corporation	Cat# 242-00087
Acetone	FUJIFILM Wako Pure Chemical Corporation	Cat# 016-00346
Critical commercial assays		
QuantiTect Reverse Transcription Kit	Qiagen	Cat# 205311
Wizard® SV Gel and PCR Clean-Up System	Promega	Cat# A9281
FastGene™ Plasmid Mini Kit	NIPPON GENE	Cat# FG-90502
PureLink™ HiPure Plasmid Midiprep Kit	Thermo-Fisher Scientific	Cat# K210005
QuikChange Site-Directed Mutagenesis Kit	Agilent	Cat# 200519
Dual-Luciferase® Reporter Assay System	Promega	Cat# E1910
Deposited data		
RNA-seq data (NASA's Rodent Research Project)	NASA	https://osdr.nasa.gov/bio/repo/data/studies/OSD-104
RNA-seq data (Mouse Habitat Unit-1 mission)	Okada et al.[4]	Accession number: DRA010983
RNA-seq data (Large Maf TKO)	This paper	Accession number: DRA014336
Experimental models: Cell lines		
AAVpro 293T Cell Line	Takara Bio	Cat# 632273
Experimental models: Organisms/strains		
Mouse: C57BL/6J	The Jackson Laboratory	RRID:IMSR_JAX:000664
Mouse: B6.Cg-Tg(ACTA1-cre)79Jme/J	The Jackson Laboratory	RRID:IMSR_JAX:006149
Mouse: $Mafa^{-/-}$	Zhang et al.[27]	N/A
Mouse: $Mafb^{flox/flox}$	Tran et al.[45]	N/A
Mouse: $Maf^{flox/flox}$	Fujino et al.[46]	N/A
Oligonucleotides		
See Table S1 for genotyping primers	This paper	N/A
See Table S1 for RT-qPCR primers	This paper	N/A
See Table S1 for cloning primers	This paper	N/A
Recombinant DNA		
pGL4.10-Myh4	This study	N/A
pGL4.10-Myh4_mut	This study	N/A
pGL4.10-Myh1	This study	N/A

(*Continued on next page*)

Continued

REAGENT or RESOURCE	SOURCE	IDENTIFIER
pGL4.10-Myh2	This study	N/A
pGL4.10-Myh3	This study	N/A
Software and algorithms		
ImageJ	NIH	https://imagej.net/software/fiji/
BIOREVO BZ-X800 microscope system	Keyence	N/A
CLC Genomics Workbench	Qiagen	RRID:SCR_011853
DAVID Bioinformatics Resources 6.8	LHRI	RRID: SCR_001881
MEME FIMO v5.5.0	Grant et al.[51]	RRID:SCR_001783
Morpheuse	Broad Institute	https://software.broadinstitute.org/morpheus
Prism v7	GraphPad	https://www.graphpad.com/
Other		
Dynamometer	Melquest	Cat# GPM101B
Treadmill	Melquest	Cat# TMS-4N
Thermal Cycler Dice® Real Time System Single	Takara Bio	Cat# TP850
NanoDrop™ 2000/2000c	Thermo-Fisher Scientific	Cat# ND-2000
GloMax® 20/20 Luminometer	Promega	Cat# E5311

RESOURCE AVAILABILITY

Lead contact

Further information and requests for reagents may be directed to and will be fulfilled by the lead contact, Ryo Fujita (fujiryo@md.tsukuba.ac.jp), or Satoru Takahashi (satoruta@md.tsukuba.ac.jp).

Materials availability

All unique reagents generated in this study are available from the lead contact in accordance with the relevant material transfer agreements.

Data and code availability

- All data that support the findings of this study will be shared by the lead contact upon request.
- RNA-seq data are deposited in The DNA Databank of Japan (https://www.ddbj.nig.ac.jp/) and are publicly available as of the date of publication. The accession number is listed in the key resources table. This paper analyzes existing, publicly available data.
- This paper does not report original code.
- Any additional information required to reanalyze the data reported in this paper is available from the lead contact upon request.

EXPERIMENTAL MODELS AND SUBJECT DETAILS

Mice

Mice were maintained under specific pathogen-free conditions in the Laboratory Animal Resource Center at the University of Tsukuba, Ibaraki, Japan. *Mafa* knockout mice were generated in a previous study.[27] Mice harboring the floxed *Mafb* and *Maf* allele were generated using a method described in our previous work.[45,46] B6.Cg-Tg(ACTA1-cre)79Jme/J (HSA-Cre79, IMSR_JAX:006149) mice were purchased from the Jackson Laboratory (Bar Harbor, ME, USA). *Mafa*$^{-/-}$::*Mafb*$^{flox/flox}$::*Maf*$^{flox/flox}$ mice were crossed with HSA-Cre79 mice to generate the skeletal muscle specific conditional knockout mice. All experiments were performed in compliance with the relevant Japanese and institutional laws and guidelines and were approved by the University of Tsukuba Animal Ethics Committee (authorization number: 21-185).

METHOD DETAILS

Data from GeneLab

Large Maf transcript data were obtained from the GLDS-104 dataset in GeneLab (genelab.nasa.gov). Spaceflight mission and experimental details for each dataset, including handling of the rodents, tissue processing, RNA extraction, and raw data pertaining to

either microarray or RNA-sequencing, can be found in the GeneLab database. Briefly, the dataset included a transcriptome analysis of the soleus muscle of mice after a 37-day space flight.

RNA-seq analysis

Total RNA was extracted from 100 sections of frozen soleus and EDL tissues sliced to a thickness of 8 μm using TRIzol reagent (Thermo Fisher Scientific, Waltham, MA, USA). The RNA-seq library was prepared using the NEBNext Ultra Directional RNA Library Prep Kit (New England Biolabs, Ipswich, MA, USA) after ribosomal RNA (rRNA) depletion (NEBNext rRNA Depletion Kit; New England Biolabs). Paired-end (2 × 36 bases) sequencing was performed using the NextSeq500 platform (Illumina, San Diego, CA, USA). FASTQ files were imported to the CLC Genomics Workbench (Version 10.1.1; Qiagen, Hilden, Netherlands). Sequence reads were mapped to the mouse reference genome (mm10). Counts were normalized with the trimmed mean normalization method (Robinson and Oshlack, 2010). Genes with 0 counts in any sample were excluded, and differential expression was analyzed using the Empirical Analysis of DGE tool (edgeR test) in CLC Main Workbench (Version 22.0; Qiagen). Differentially expressed genes were extracted among conditions (WT_EDL vs TKO_EDL, WT_Sol, TKO_Sol) with a false discovery rate–corrected $P < 0.05$. DAVID Bioinformatics Resources 6.8[47] was used for gene ontology analysis with P-value < 0.05.

Quantitative analysis of transcripts using reverse transcription PCR

Total RNA was extracted from various tissues and hindlimb muscles using ISOGEN (NIPPON GENE, Chiyoda, Tokyo, Japan). First-strand cDNA was synthesized using the QuantiTect Reverse Transcription Kit (Qiagen). Polymerase chain reaction (PCR) was performed using a THUNDERBIRD SYBR qPCR system (Toyobo, Osaka, Japan) and a TP850 Thermal Cycler Dice Real Time System (Takara Bio, Kusatsu, Japan). The primer sequences are listed in Table S1. The relative amount of each transcript was normalized to the amount of *TATA-box-binding protein* (*Tbp)* transcripts.

SDS-PAGE

Myofibrillar-rich proteins were extracted from soleus and EDL muscles, as previously described.[48] The total protein concentration (A280) was measured using a NanoDrop 2000 Spectrophotometer (Thermo Fisher Scientific). Protein samples (2 μg/well) were separated using SDS-PAGE on a 7.5% polyacrylamide gel at a constant voltage of 80 V for 20 h at 22-26°C. The gel was then stained with CBB G-250 stain (Bio-Rad) for 1 h at 22-26°C. Quantification of the stained bands was performed using ImageJ software (NIH, Frederick, MD, USA).

Histological analysis and immunohistochemistry of muscle cryosections

The Achilles tendon side of each hindlimb muscle was vertically mounted on tragacanth gum (Wako, Osaka, Japan) on a cork disc and quickly frozen in isopentane cooled in liquid nitrogen. Frozen tissue sections (8 μm in thickness) were mounted on glass slides.

For hematoxylin/eosin staining, sections were stained with Mayer's hematoxylin (Wako, Osaka, Japan) for 7 minutes. After washing in warm running tap water (50 ± 5°C) for 3 minutes, the sections were stained with eosin (Wako, Osaka, Japan) for 50 seconds, then dehydrated by 2 changes (5 seconds each) of 95% ethanol and 2 changes (5 seconds each) of 100% ethanol (Wako, Osaka, Japan), and finally cleared with 3 changes of xylene (Wako, Osaka, Japan) for 5 minutes each. The sections were mounted with DPX mounting medium (Sigma-Aldrich). All samples were observed with a BIOREVO BZ-X800 microscope.

For SDH staining, sections were incubated with a SDH solution (0.2 M sodium succinate, 0.2 M phosphate buffer pH 7.4, nitro-blue tetrazolium) for 30 minutes at 37°C. To dehydrate and remove unbound nitro-blue tetrazolium, the sections were then placed into different acetone solutions for 3 seconds in the following order: 30% → 60% → 90% → 60% → 30%. After washing with running tap water, the sections were mounted with glycerol gelatin (Sigma-Aldrich). All samples were observed within 2 hours of the staining procedure, and intensities were measured using Image J software (National Institute of Health).

The sections for immunohistochemical analysis were fixed with −20°C acetone and air-dried. After blocking with 5% goat serum/1% BSA/phosphate-buffered saline (PBS) and M.O.M. blocking reagent (Vector Laboratories, Newark, CA, USA), the samples were incubated with primary antibodies overnight at 4°C. Antibodies are listed in key resources table. All immunostained samples were visualized using appropriate Alexa Fluor conjugated secondary antibodies (Thermo Fisher Scientific) for 1 h at 37°C. Tissue sections were mounted with VECTASHIELD Vibrance Antifade Mounting Medium (Vector Laboratories). The proportion of each myofiber type and the CSA of myofibers were assessed using images captured with a BIOREVO BZ-X800 microscope system and hybrid cell count application (Keyence, Osaka, Japan). Myofibers were counted in Sol, Pla, Gas, TA, and EDL muscle samples in a total of 358-730, 349-1176, 2058-3819, 1199-2221, and 494-1004 myofibers per section, respectively.

Grip strength test

Forelimb grip strength was determined using a dynamometer (GPM-101B; Melquest, Toyoma, Japan).[49] The forepaws of mice were allowed to grab a horizontal bar and the tail was slowly pulled back by a researcher. Tension was recorded from the gauge at the time the mouse released its forepaws from the horizontal bar. Measurements were repeated ten times, and mean tension from the ten measurements was used in analyses.

Treadmill test

Mice (15–16 weeks of age) were subjected to a low-intensity run-to-exhaustion protocol on a motorized treadmill, as described previously.[50] Mice were familiarized with the treadmill (Melquest) for 10 min at 10 m/min for two consecutive days. The following day, mice were set to run at 10 m/min for 30 min, 11 m/min for 15 min, and 12 m/min for 15 min. Finally, the speed was incrementally increased by 1 m/min every 10 min until the mouse exhibited exhaustion. The endpoint was reached when the mouse sat on the shock grid at the back of the treadmill and stopped responding to continuous tail brushing for 20 s.

Transmission electron microscopy

EDL muscle samples were pre-fixed in 2.5% glutaraldehyde/0.1 M phosphate buffer for 2 h at 4°C, then post-fixed in 1% osmium tetroxide for 30 min at 4°C, as described previously.[51] After dehydration in ethanol, the samples were embedded in Epon (Polysciences). The longitudinal thin-sections were double-stained with uranyl acetate and lead citrate and examined under a JEM1400 transmission electron microscope (Jeol, Tokyo, Japan). Quantitative examination of mitochondria and area was performed using Image J software (National Institute of Health). Five or six images per mouse were analyzed at 3,000× magnification and the areas were converted to μm^2 through the division of the number of pixels by the scale bar.

Motif enrichment analysis

Presence of MARE sites in the promoter regions of genes were predicted using the FIMO (Find Individual Motif Occurrences) algorithm from the MEME Suite,[51] using the position weight matrix available from JASPAR (https://jaspar.genereg.net/). This analysis was run from 3 kb upstream to 3 kb downstream of transcriptional start site of *Myh4*.

Luciferase assay

The 500 bp 5′ upstream region (−450 to +50) of *Myh4* from gastrocnemius muscle DNA of C57BL/6 mice was inserted into a pGL4.10 promoter-less luciferase vector (Promega, Madison, WI, USA) and named pGL4-Myh4. Specific mutation of the putative MARE sequence was generated using the QuikChange Site-Directed Mutagenesis Kit (Agilent Technologies, Santa Clara, CA, USA) (pGL4-Myh4_mut). The primer sequences for the construction of vectors are shown in Table S1. To examine whether Mafa, Mafb, or Maf could activate the Myh4 promoter, either pGL4-Myh4 (100 ng) or pGL4-Myh4_mut (100 ng) was co-transfected with pRL-TK vectors (50 ng, Promega) and the pcDNA3.1-large Mafs expression vectors (0 ng, 100 ng, 200 ng) into AAVpro 293T cells (Takara Bio) using the FuGENE HD transfection reagent (Promega). Twenty-four hours after transfection, the cells were harvested and assayed using the Dual-Luciferase Reporter Assay System (Promega). Luciferase activity was measured by GloMax® 20/20 Luminometer (Promega) and was normalized on the basis of *Renilla* luciferase activity from the pRL-TK vector. The promoter regions of *Myh1*, *Myh2*, and *Myh3* were examined as negative controls.

AAV-mediated skeletal muscle Mafa/Mafb/Maf overexpression

Mafa, Mafb, and *Maf* genes were amplified by PCR from cDNA of pancreas, kidney, and eye, respectively, using primers listed in Table S1, then cloned into a pAAV-CMV vector (serotype 6, AAV6) using the In-Fusion Cloning HD Kit (Takara Bio). AAV6 particles were generated with the Helper Free System (Takara Bio, 6651). AAVpro 293T cells (Takara Bio, 632273) were seeded in 100 mm dishes (2×10^6 cells per dish) with PEI (polyethylenimine) Max medium (Polysciences, Warrington, PA, USA) and plasmids for the following: pRC6 and pHelper along with pAAV-CMV-Mafa-flag, -Mafb-flag or -Maf-flag. The medium was harvested 72 h later and purified with an AAVpro Purification Kit (Takara Bio, 6666) and titer was calculated using AAVpro® Titration Kit (for Real Time PCR) Ver.2 (Takara Bio, 6233). Randomized 11-week-old WT mice were injected in the soleus muscle with 4.0×10^9 particles of AAV-Mafa, -Mafb, or -Maf in 100 μL. AAV-Mafa were injected into the TA muscle of 11-week-old TKO mice with 2.5×10^9 particles in 100 μL. Control mice were injected with the same amount of saline. The muscles were collected eight weeks after injection.

QUANTIFICATION AND STATISTICAL ANALYSIS

Graphs are presented as mean ± SEM, as indicated in Figure legends. Significance was calculated using GraphPad Prism software by either Student's t-test or one-way ANOVA with Tukey's test: *P < 0.05, **P < 0.01, ***P < 0.001, ns, not significant.